Materials and Design 44 (2013) 35–48

Contents lists available at SciVerse ScienceDirect

Materials and Design

journal homepage: www.elsevier.com/locate/matdes

Ballistic resistance of high hardness armor steels against 7.62 mm armor piercing ammunition

Namık Kılıç [a,*], Bülent Ekici [b]

[a] Computer Aided Engineering Department, Otokar Otomotiv ve Savunma San, A.S, Atatürk Cad No: 9 Arifiye, 54580 Sakarya, Turkey
[b] Department of Mechanical Engineering, Faculty of Engineering, Marmara University, Istanbul 34722, Turkey

ARTICLE INFO

Article history:
Received 9 May 2012
Accepted 15 July 2012
Available online 28 July 2012

Keywords:
Ballistics
High hardness steel
Armor piercing bullet
Smoothed particle hydrodynamics
Lagrange
Numerical simulation

ABSTRACT

Although advanced lightweight composite based armors are available, high hardness steels in military vehicles are often used to provide ballistic protection at a relatively low cost and is an interesting material due to its widespread usage in vehicle structure. In this study, ballistic limit of 500 HB armor steel was determined against 7.62 mm 54R B32 API hardened steel core ammunition. Lagrange and smoothed particle hydrodynamics (SPH) simulations were carried out using 3D model of bullet and high hardness armor target. Perforation tests on 9 and 20 mm thickness armor were performed to validate simulation methodology. Also material tests were performed for armor steel and ammunition hardened steel core to develop Johnson–Cook constitutive relations for both strength and failure models. Finally, results from 3D numerical simulations with detailed models of bullet and target were compared with experiments. The study indicates that the ballistic limit can be quantitatively well predicted independent of chosen simulation methodology, but qualitatively some differences are seen during perforation and fragmentation. As shown in results, good agreement between Ls-Dyna simulations and experimental data was achieved by Lagrange formulation with the full bullet model.

1. Introduction

High velocity impact and penetration problems include large deformation, erosion, high strain rate dependent nonlinear material behavior and fragmentation. Therefore, it is important to model mechanical behavior of the penetration where above affects are taken into account. In reality since empirical and analytic approaches cannot capture all of multiple physical phenomena including fracture, failure, residual stresses and friction heating [1,2], numerical simulation has become a necessary tool for the ballistic penetration study. Numerical methods and corresponding computing technologies have been evolved to the level where mentioned complex deformation and penetration pattern during ballistic impact can be accurately predicted. The usage of numerical methods in the development of design alternatives will not only introduce shorter armor development time, but also will reduce the number of prototypes to minimize the number of the real scaled field tests required, and also help us to visualize the impact behavior.

A review of the literature on impact simulations show that the most research in this field have been focused on the development and application of continuum hydro-codes using either mesh based Lagrangian or mesh free formulations [3–6]. Lagrange formulation is widely used because of its advantages, such as low level of computational cost, being able to track accurately and efficiently material interfaces and incorporate complex material models [7]. Accurate and realistic simulation of ballistic penetration with Lagrange formulation requires complicated contact and erosion algorithms. However, it is very sensitive to distortions resulting small time steps and possible loss of accuracy. The well known negative volume errors occur as a result of such mesh tangling issues. Numerical codes can handle these problems with adaptive re-meshing algorithms or by eroding the highly distorted elements with artificial manipulation which can cause loss of accuracy. On the other hand, high computational cost of adaptive remeshing algorithms and its limited applicability on three dimensional problems decrease the attractiveness. As an alternative to mesh based Lagrangian formulation, smoothed particle hydrodynamics is a meshless computational technique, which has some special advantages over the traditional mesh-based numerical methods. Because of the adaptive nature of the SPH approximation, it can handle problems with extremely large deformations very well [8]. The SPH particles also carry material properties, functioning as both approximation points and material components. These particles are capable of moving in space, carry all computed information, and thus form the computational frame for solving the partial differential equations describing the conservation laws. In

* Corresponding author. Tel.: +90 264 229 22 44x5400; fax: +90 264 229 22 42.
E-mail address: nkilic@otokar.com.tr (N. Kılıç).

0261-3069/$ - see front matter © 2012 Elsevier Ltd. All rights reserved.
http://dx.doi.org/10.1016/j.matdes.2012.07.045

application, the principal potential advantage of the SPH method is that there is no need for connectivity between particles with a conventional mesh, hence avoiding element distortion problems at large deformations [9].

A popular explicit code, Ls-Dyna was successfully used to simulate several types of armors subjected to impact ammunition for various threat levels and capable of applying both Lagrange and SPH methods. Earlier studies on steel plates impacted by various projectiles [10–17] show that, ballistic penetration behavior can be simulated using either Lagrange or SPH. Borvik et al. [12] considered ballistic penetration performance of five different steel alloys, yield strengths ranging from 600 to 1700 MPa with Lagrange discretization. They demonstrated that, compared experimental and numerical studies show reasonable agreement in determination of ballistic limit velocity. There is almost a linear correlation between ballistic limit velocity and yield strength and for BR7 level armor piercing ammunition yield strength shall be around 1500 MPa for 12 mm target. Dey et al. have been studied ballistic perforation resistance of 12 mm Weldox 700 steel targets with gas gun fired ogival projectiles which have 52 HRc hardness. Although comprehensive strength and failure models were given for armor plate, hardened steel projectile was modeled as an elastic–plastic material with bilinear isotropic hardening without fracture [13,15]. Fountzoulas et al. [18] studied tungsten carbide sphere impact on HSLA-100 including both SPH and Lagrange methods and conclude that Lagrange is more successful in steel target modeling. A similar outcome for SPH also derived by Buyuk et al. [19] In their study deformation pattern of thin aluminum folio against 9 mm Nato ball bullet was studied both experimentally and numerically. SPH results were found to be similar in behavior but poor in magnitude. Mostly, SPH methodology is used to model ceramic targets in ballistic simulation due to its enhanced sensitivity to spall formation.

In this paper, ballistic limit thickness for Secure 500 was determined against 7.62 mm 54R B32 API hardened steel core ammunition using both Lagrange and smoothed particle hydrodynamics SPH simulations. The parameters related with numerical modeling such as mesh size, contact algorithms are validated with perforation tests on 9 and 20 mm thickness. Also material tests were performed for armor steel and ammunition hardened steel core to develop Johnson–Cook constitutive relations for both strength and failure models. Material data for the bullet jacket and sabot were mainly taken from literature. Finally, results from 3D numerical simulations with detailed models of bullet and target were tabulated to find minimum ballistic thickness against Stanag 4569 level 3 threats.

2. Material behavior and modeling

In order to describe multiple physical phenomena taking place during high velocity impact and penetration, it is required to characterize the behavior of materials under high strain rate loading conditions. The material behavior model includes not only the stress–strain relationship at large strains or different strain rates but also accumulation of damage and mode of failure. Such complex material behavior including fracture is difficult to characterize in analytical models but in numerical simulations, complex constitutive materials models can be implemented. A widely used material model in ballistic penetration studies which also available in commercial hydro-codes is Johnson–Cook. The Johnson–Cook model is a visco–plastic model for ductile metals that consider strain hardening, strain rate and thermal softening effects on material behavior and fracture [20]. This model is widely used since its first publication in 1983. For many materials, J–C parameters can be easily found in open literature. In spite of parameters availability for many materials, when ballistic application is the subject of study, not a lot of publications give their material parameters or share rather general parameters taken from open literature. For this reason, in the characterization of materials for simulation, deriving experiment based models is crucial part of the study.

Johson–Cook expresses the equivalent stress as a function of plastic strain, strain rate and temperature with an empirical relationship for the flow stress, which is represented as [20].

$$\sigma_Y = \left[A + B\varepsilon_p^n\right]\left[1 + C\log\dot{\varepsilon}_p^*\right]\left[1 - T_H^m\right] \tag{1}$$

where ε_p is the equivalent plastic strain, $\dot{\varepsilon}_p^*$ is the dimensionless plastic strain rate for $\dot{\varepsilon}_0$, T_H is homologous temperature $\{T_H = (T - T_{\text{room}})/(T_{\text{melting}} - T_{\text{room}})\}$. The five material constants are A, B, C, n and m. The expression in the first set of brackets gives the stress as a function of $\dot{\varepsilon}_p^* = 1$ and $T_H = 0$. The expression in the second and third sets of brackets represent the affects of strain rate and thermal softening respectively.

In order to describe ductile fracture, Johnson and Cook also proposed a model including the effects of stress triaxiality, temperature, strain rate on failure strain. The Johnson–Cook damage model is a cumulative damage – fracture model that takes into account the loading history, which is represented by the strain to fracture. In other words, model assumes that damage accumulates in the material during plastic straining and the material breaks immediately when the damage reaches a critical value. This means the damage has no contribution on the stress field until the fracture happens. The strain to fracture is expressed as a function of strain rate, temperature and pressure. Parameters of strain hardening D_1,D_2 and D_3 are predominant compared with two others strain rate hardening and thermal softening, therefore should be found out carefully. J–C is an instantaneous failure model, which means no strength remains after erosion of an element. The damage of an element is defined on a cumulative damage law:

$$D = \sum \frac{\Delta\varepsilon}{\varepsilon^f} \tag{2}$$

in which

$$\varepsilon^f = [D_1 + D_2\exp(D_3\sigma^*)]\,\lfloor 1 + D_4\ln|\dot{\varepsilon}_p^*|\rfloor\,[1 + D_5 T_H] \tag{3}$$

The dimensionless pressure/stress ratio (σ^* is the ratio of hydrostatic stress per effective stress) is a measure of triaxiality of the stress state and defined as

$$\sigma^* = \frac{\sigma_H}{\sigma_{eq}} = \frac{(\sigma_x + \sigma_y + \sigma_z)/3}{\sqrt{\sigma_x^2 + \sigma_y^2 + \sigma_z^2 - \sigma_x\sigma_y - \sigma_y\sigma_z - \sigma_z\sigma_x + 3(\tau_{xy}^2 + \tau_{yz}^2 + \tau_{zx}^2)}} \tag{4}$$

The damage variable D take values between 0 and 1, here $D = 0$ for an undamaged material and failure of the elements assumed to occur when $D = 1$. The failure strain and thus the accumulation of damage is a function of mean stress, strain rate and temperature.

2.1. Armor plates

The armor material used in ballistic tests is an alloyed, liquid-quenched and tempered high-strength special steel for civil use which has 500 HB hardness. The material properties tabulated for transverse specimens according to EN 10002 in Table 1.

The data obtained from laboratory tests are grouped in two types. First test series consisted of the quasi-static tests at large strains performed at room temperature. Four various strain rates were performed 10^{-4}, 10^{-3}, 10^{-2} and $0.1\,s^{-1}$ on two type smooth flat specimens taking length to cross section ratio as 2. All the tensile

Table 1
Mechanical properties for 500 HB armor steel.

Hardness in Vickers	Min tensile strength (MPa)	Min yield strength (MPa)	Min elongation at break (%)
480–530	1600	1300	9

tests were peformed with the specimens manufactured in tranverse with respect rolling direction.

The yield stress parameter A and the hardening parameters B and n for the J–C constitutive relation in Eq. (1) were determined from the quasi-static tensile tests. Fig. 1 shows the measured quasi-static true stress strain curves for armor material until the fracture. The stress is based on continous measurement of applied load and current area of the specimen using video extentiometer. In the regions showed with square, the true stress–strain values are not exact values due to necking. During necking of the specimens at large strains, there is a component of hydrostatic tension that tends to make the total tensile stress greater than equivalent stress. Therefore in model development, the values up to maximum tensile strength are taken into account. In order to determine the strain and strain rate hardening parameters "c" and "n", 3 and 4 mm diameter cylindrical specimens used in Split Hopkinson pressure bar (SHPB) test setup. Preliminary ballistics simulation studies with Ls-Dyna have shown that, during penetration mostly strain rates are around 1000 s^{-1}. Therefore during model development, strain rates 420, 780, 1050 and 1250 s^{-1} generated on specimens to establish strain rate dependency. In order to control strain rate also 10, 15 and 30 mm length specimens with various cross-section diameter were used.

For continuously increasing deformation rates, rate value is specified just after necking, for constant rates, mean value was taken. As shown in graphics (see Fig. 2a–d), the necking is decreasing with increasing deformation rates. In the tests, the stress–strain relationship and fracture strains obtained for a wide range of strain rates but temperature was kept constant. In Fig. 3a, developed model was compared with test results. For lower plastic strains, the correlation between model and test results is good. With increasing strain rates, even at higher plastic strains, the correlation between model and test results is reasonable to use in simulations. During tests, failure strain is collected at various deformation rates ranging from quasi-static to high rates such as 1000 s^{-1} and a linear curve fit established as shown in Fig. 3b.

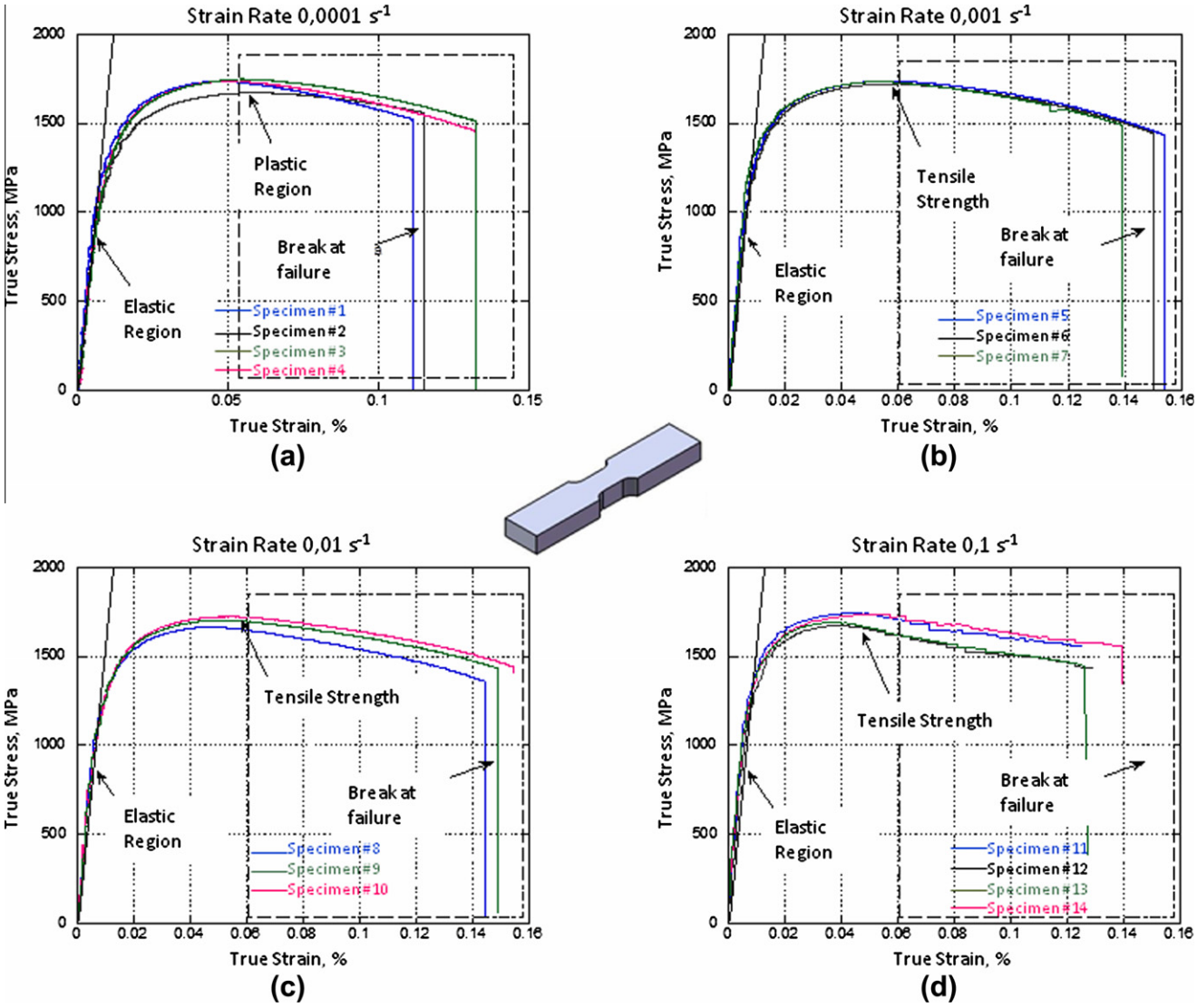

Fig. 1. Quasi-static tensile tests for armor material for various strain rates: (a) 1×10^{-4}, (b) 1×10^{-3}, (c) 1×10^{-2} and (d) 1×10^{-1}.

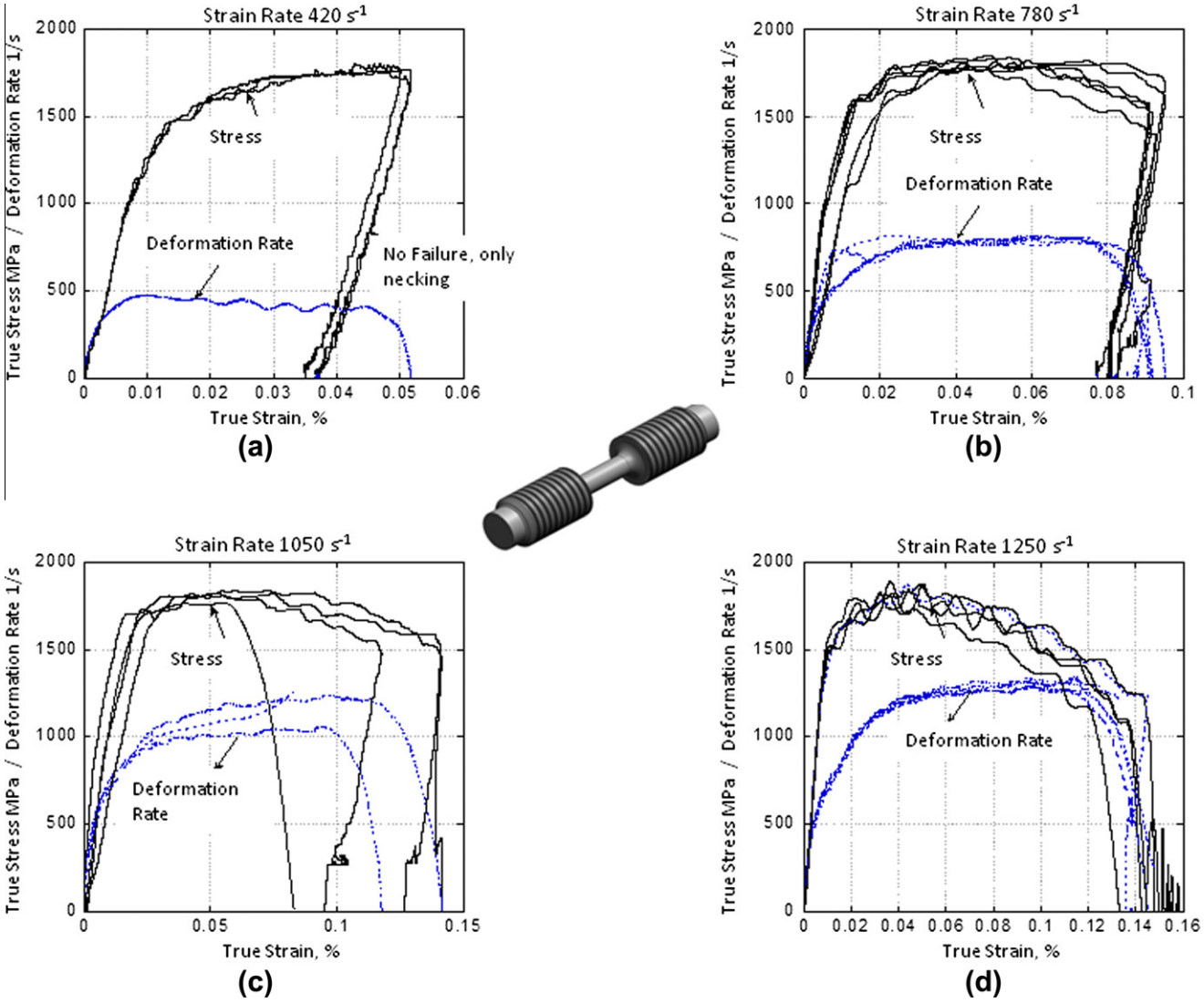

Fig. 2. SHPB high strain rate test results for various strain rates: (a) 420 s^{-1}, (b) 780 s^{-1}, (c) 1050 s^{-1} and (d) 1250 s^{-1}.

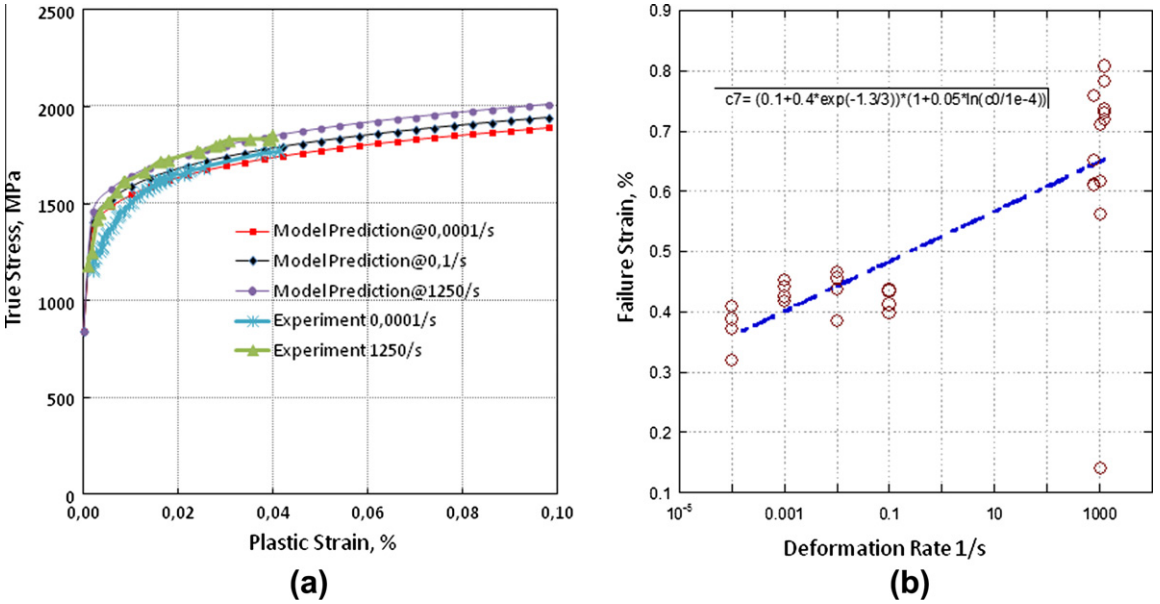

Fig. 3. J–C constitutive model comparison: (a) with test results for various strain rates and (b) failure parameters curve fit with test results.

Table 2
J–C constitutive model constants for target material.

Strain hardening			Strain rate hardening		Temp. softening
A (MPa)	B (MPa)	n	c	$\dot{\varepsilon}_0$ (s^{-1})	m
1270	1580	0.175	0.0038	10^{-4}	1
D_1	D_2	D_3	D_4	$\dot{\varepsilon}_0$ (s^{-1})	D_5
0.1	0.4	−1.3	0.05	10^{-4}	0

J–C flow and failure parameters for target material are tabulated in Table 2. In literature mostly notched cylindrical specimens were used to determine failure parameters and triaxiality dependence, in this study parameters determined with least squares curve fitting approach. Thermal softening parameter "m" is taken as unity to identify linear temperature dependence without performing any tests. Borvik et al. [12] has also chosen "m" as unity for high hardness steels and Kurtaran et al. [21] has chosen "m" as 1.03 for 4340 steel.

In open literature, there are a few J–C parameters available which have hardness around 500 BHN. One of the studies about Armox 500 manufactured by SSAB (mechanical properties are close to armor used in this study) has been performed by Skoglund and Nilsson [22,23]. They have found that $A = 1470$ MPa, $B = 702$ MPa, $n = 0.199$, $c = 0.00549$ and $m = 0.811$. The failure parameters were found to be $D_1 = 0.068$ $D_2 = 5.382$ and $D_3 = -2.554$. The material stress flow results at 1000 s^{-1} strain rate are matched with Skoglund ignoring temperature dependence. Nsiampa [24] has reported J–C parameters for a similar hardness material also. In Table 3, a list of J–C parameters found in literature for 500 HB steels are tabulated.

2.2. Hardened steel core projectile

In this study, 7.62 mm armor piercing ammunition is used for protection level 3 according to Stanag 4569. Material data for the armor piercing bullet is generally not available in the literature and is extremely difficult to make specimens for material testing directly from the ammunition. Buchar et al. [10] Borvik et al. [12] and Chocron et al. [25] have been reported some tensile material test data or J–C parameters for the hardened steel core. Although, it is difficult to make specimens for material testing directly from bullet parts, miniature specimens prepared from cylindrical part of hardened steel core (see Fig. 4). Even in low strain rate tests, due to machining faults, most of the failures happened at the thread interfaces. In order to eliminate early failures before plastic strain occurs, various specimen types were used in both tensile and compression tests.

The quasi-static stress–strain response was measured for the steel core material. Tensile specimens were machined, instrumented with strain gauges and strained until failure. The test results are plotted in Fig. 5 a and b. It was found that the core material fails at stress of 2.3 GPa with 2–3% plastic strain. This information coincides with the tensile strain–stress response Chocron has found [25].

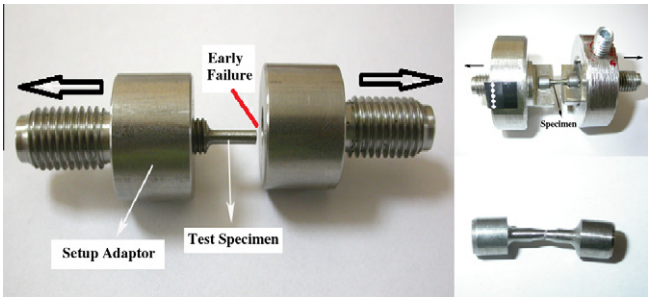

Fig. 4. Notched dynamic test specimens.

However, there is high variation in strain to failure and associated ultimate stress. As shown in Fig. 6, J–C constitutive parameters were derived from experimental results using curve fits and tabulated in Table 4.

Due to the difficulties experienced during specimen preparation and early failure without achieving plastic strain during tests, a comperative study with the literature based material models would increase confidence level before simulation. At least, a hardness measurement will establish a base to make a comment about mechanical properties found. Vickers hardness (HV) of the bullet core material first determined (see Fig. 7a). Unfortunately it is difficult to correlate HV numbers to material properties but a rough estimation suggests that, the ultimate tensile strength is about three times the Vickers hardness number. That means that, UTS is around 2500 MPa, which coincides with Buchar et al. [10], Borvik et al. [12] and Niezgoda Morka [26]. J–C model parameters for 7.62 armor piercing ammunition steel core found by experimentally are compared with the open literature and tabulated in Table 5.

Borvik et al. [12] has modeled 7.62 AP bullet steel core around 1200 MPa yield strength but extremely high strain hardening parameters and without any strain rate hardening. The simulation results are close to model the steel core as rigid. He also eliminated failure parameters. The hardened steel core is often modeled as rigid body but simulations have shown this may increase penetration depth because some plastic deformation always takes place. In shot tests, frequently hardened steel core broke into two pieces but not a significant plastic deformation occured. The initial results were disappointing for the hardened steel core AP ammunition. The bullet appeared to be eroded prematurely and the penetration depth results are underestimated for 20 mm target (Fig. 7b). Contrary to the simulations, in tests, the hardened steel core is not eroded and do not have significant deformation on tip. (Fig. 15) In order to improve predictions dynamic yield strength of bullet increased by changing strain hardening coefficient. After increasing value "c" to 0.05 the results become more realistic and predict the depth of penetration with reasonable approximation.

2.3. Equation of state

The relation between pressure, volume and internal energy of a material is defined as the equation of state. Zukas et al. [2] indicated that for solid–solid impacts in the 500–2000 m/s velocity

Table 3
J–C constitutive model constants for 500 HB steel.

	Hardness	Yield (MPa)	Tensile (MPa)	Strain hardening			Strain rate hardening		m
	HB			A (MPa)	B (MPa)	N	c	$\dot{\varepsilon}_0$ (s^{-1})	
Domex protect 500 [12]	477–550	1500	1800	2030	504	1	0.001	5e-4	1
Armox 500T [22]	480–540	1250 min	1450–1750	1470	702	0.199	0.0054	1	0.811
Armox 500T [23]				849	1340	0.092	0.0054	–	0.87
Secure 500 [24]	480–530	1300	1600	1299	2230	0.5585	0.04447	–	0.961

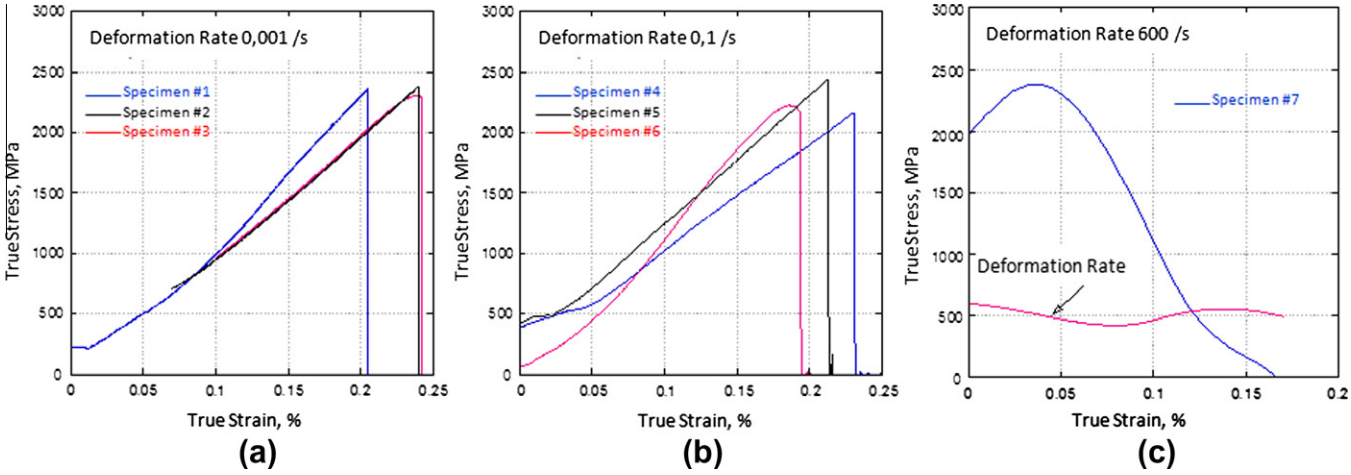

Fig. 5. AP bullet tensile test results: (a) quasy-static at deformation rate 0.001 s^{-1}, (b) 0.1 s^{-1} and (c) dynamic test results at 600 s^{-1}.

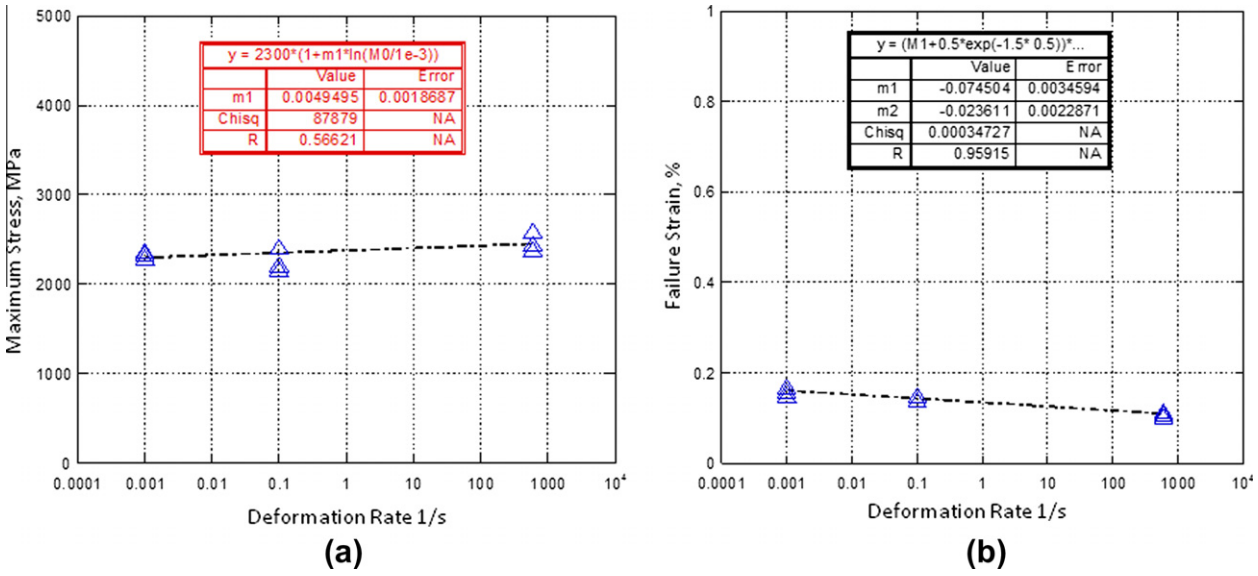

Fig. 6. J–C constitutive parameters curve fit: (a) strength flow and (b) failure.

regime, only moderate pressures are generated and this decays rapidly to the values comparable to the strength of the material. Therefore the EOS in the impact calculations is of secondary importance. Many researchers have been used linear polynomial EOS by using bulk modulus only factor in relation of pressure and volumetric strain. Although it seems appropriate for weak shocks, preliminary simulations with linear polynomial EOS show poor approximation in both penetration depth and crater formation. In contrary to the general expectation, Ls-Dyna theory manual [3] does not recommend to use linear polynomial EOS beyond the elastic regime. Further literature survey on ballistic impact studies indicates that using nonlinear EOS [27–29] had provided good agreement between numerical and experimental results. In this numerical modeling, Mie-Gruneisen equations of state is used.

$$P = \frac{\rho_0 C^2 \mu(1 + (1 - \gamma/2)\mu - (\alpha/2)\mu^2)}{[1 - (S_1 - 1)\mu - S_2\mu^2/(\mu + 1) - S_3\mu^3/(1 + \mu)^2]} + (\gamma + \alpha\mu)E_0 \quad (5)$$

where E_0 is the internal energy per unit volume, C is the intercept of the shock and particle velocity curve, S_1, S_2, S_3 are the cofficients of the slope of the shock and particle velocity curve, γ is the Gruneisen coefficient. α is the volume correction factor and $\mu = \rho/\rho_0 - 1$ is the compression factor. The Mie Gruneisen EOS data for AP bullet is taken from Niezgoda and Morka [26] for 62 HRc penetrator, EOS parameters for the target plate is taken from Gailly and Espinosa [29] as RHA steel.

Table 4
J–C constitutive model material constants for ammunition hardened steel core.

Strain hardening			Strain rate hardening		Temp. softening
A (MPa)	B (MPa)	n	c	$\dot{\varepsilon}_0$ (s^{-1})	m
Stress flow model					
1900	1100	0.3	0.005	10^{-3}	1

3. Numerical modeling

3.1. Lagrangian method

In determination of ballistic limit thickness for high hardness armor plates against AP projectiles, three separate simulation

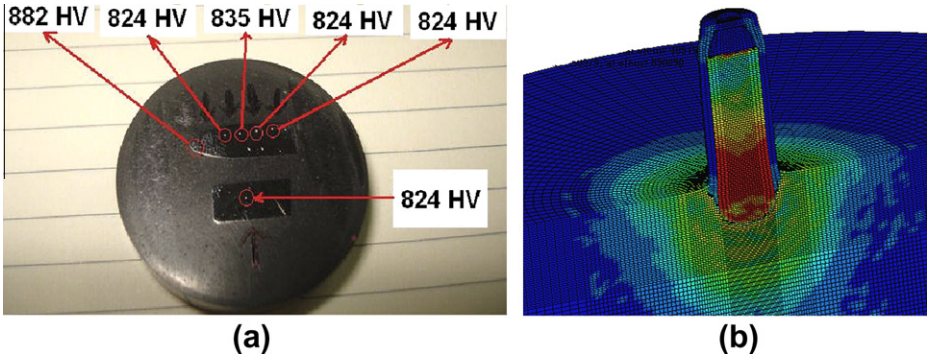

Fig. 7. AP projectile J–C model verification: (a) Vickers hardness measurement and (b) simulation results.

Table 5
Comparison of 7.62 AP steel core J–C model parameters with literature.

	Strain hardening			Strain rate hardening		m
	A (MPa)	B (MPa)	n	c	$\dot{\varepsilon}_0$ (s^{-1})	
Own	1900	1100	0.3	0.005	10^{-3}	1
Buchar et al. [10]	1650	807	0.1	0.008	n/a	1
Borvik et al. [12]	1200	50,000	1	0	5×10^{-4}	1
Niezgoda and Morka [26]	2700	211	0.065	0.005	n/a	1.17

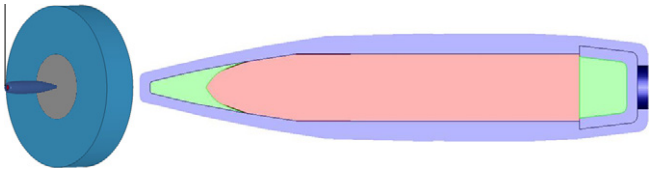

Fig. 8. Geometric model of simulation and cross-section of AP ammunition.

methodologies were used. In preliminary analysis, a 3D model was generated in Ls-Dyna for bullet assembly and target. The geometric model shown in Fig. 8, consists of an armor steel target and Stanag 4569 level 3 7.62 × 54R AP ammunition. For the AP bullet, the ogival nose hardened steel core inserted in a sabot, before the jacket is clamped onto it. In front of the core, a cap of lead–antimony is placed. The purpose of this cap is to stabilize the projectile during flight and in the initial stage of penetration.

The total mass of AP bullet is about 10.04 g. The muzzle velocity of the ammunition is 854 m/s as specified in Stanag 4569. The simulation will use the Lagrange method for ammunition and steel armor target. During solution domain generation, two different approaches were applied. In the first approach although the tip of the hardened steel core is sharp, a small radius introduced for smooth mesh generation which is shown in Fig. 9a. In second approach, tip of the steel core is modeled keeping the original geometry. Although fine mesh structure prepared, the type (a) solution domain has not achieved good correlation with test results. In type (b), due to tetragonal mesh, error termination due to element distortion would appear. In order eliminate mesh tangling issues the tip of the ogival nose is modeled with rigid elements. Since the nose is not deformed during shot tests, the rigid modeling approach for

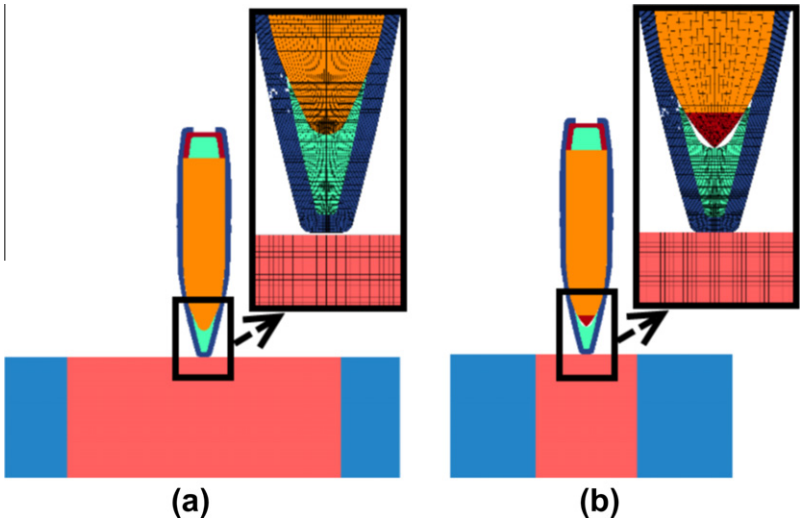

Fig. 9. Hardened steel core mesh structure: (a) smoothed radius nose and (b) sharp nose.

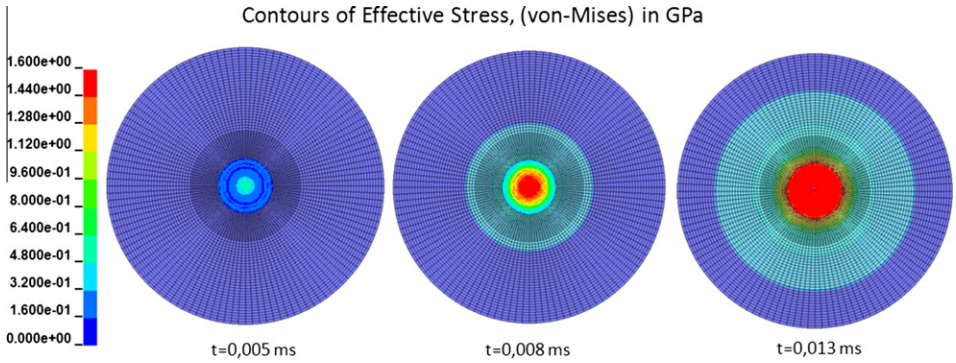

Fig. 10. Stress wave propagation through SPH-Lagrange interface.

bullet tip will not cause significant effect on penetration. (see Fig. 16)

The created FE model is optimized for the numerical stability and accuracy of results. The numerical cost of simulations is ignored and accuracy is taken as main objective of the study. The circular plate is divided into three mesh regions in radial direction; inner, middle and outer. The mesh is coarsening from inner to outer region. The mesh transition between regions is good enough to prevent stress wave reflections at the boundaries. The plate is meshed with hexagonal constant stress solid elements of varying size between 0.2 and 1 mm and total number of elements is 734.000. The projectile has also very fine mesh. The plate-bullet FE mesh includes total 941.00 elements, 207.000 elements for the bullet. Except front and rear lead–antimony caps, J–C model properties are assigned to all material. The lead–antimony caps are modeled with material card ISOTROPIC-ELASTIC-FAILURE. In FE analysis, ERODING_NODES_TO_SURFACE and ERODING_SINGLE_SURFACE contact algorithms are implemented to simulate contact between surfaces during penetration. Erosion option, dynamic and static friction and bucket sort frequency are investigated for accuracy. Control parameters are also used to control hourglass, termination of solution, time step size, contact and degree of the accuracy of the calculations. One of the most important control tools in impact problems is time step scale factor. [3] TSSF is used to provide optimum time step to confirm numerical stability. Ls-Dyna has default value of 0.9 but in these analysis 0.2 was chosen. Also in order to eliminate zero energy deformation, hourglass parameters were used to control simulation. Other control factors were chosen by default. FE simulations were conducted on a high performance compute cluster which consists of 56 CPU. Initial 3D simulations were conducted for the impact of the AP bullet against 20 mm thickness target of high hardness steel and the initial projectile velocity of 854 m/s.

3.2. SPH method

With the recent developments, SPH method became a reliable tool providing accurate and stable results for large deformation problems and successfully implemented in many commercial hydro-codes. One of FE codes which also includes SPH is Ls-Dyna. In this study, due to high computational cost of SPH, an alternative numerical solution technique of coupling FEM/SPH is used. Since SPH uses a Lagrangian formulation, a coupling between SPH and Lagrangian mesh is possible with defining contact interfaces. Similar approach has been used by Aktay et al. [17] and Azevedo and Alves [30]. The compatibility between SPH with the FE Lagrangian solver in Ls-Dyna is ensured by enabling the use of classical keywords and making easier the use of mixed approach. For impact problem, the large deformation section of the target is modeled with SPH and where the small deformation occurs is modeled with hexagonal Lagrangian solid elements. Such coupling should be carefully arranged to simulate transition of wave propagation at SPH–Lagrange interface. In Fig. 10 stress wave propagation after bullet impact is plotted at various time steps. As shown there is not a reflection at the mesh transition boundaries. The simulation will use the Lagrange method for hardened steel core projectile, SPH and Lagrange discretization for steel armor target.

The circular Lagrange layers of the armor are divided into two regions. In radial direction mesh is gradually coarsening from inner to outer. In SPH section of armor, as shown in Fig. 11 an equispaced discretization was applied. In simulations, gradually coarsening SPH discretization also applied but the results are not improving the accuracy, therefore omitted. Using the geometry detailed above a full model was generated for the analysis. The target core is modeled as SPH with particle size of 0.2 and surrounding Lagrange regions are modeled with elements size of 0.5 and 1 mm. The bullet is modeled with 3744 Lagrange solid elements and target is modeled with 144.000 Lagrange and 786.000 SPH elements. The contact between SPH and Lagrange elements is developed using CONTACT_TIED_NODES_TO_SURFACE. The contact during the penetration of bullet into target is achieved using ERODING_NODES_TO_SURFACE. In SPH simulations, the artificial bulk viscosity ignored.

In modeling, a state art rule of each FE mesh of bullet tip is in contact with at least 4 SPH nodes. Decreasing the number of SPH particles will lead to premature penetration of particles into FE mesh without carrying the material properties. Even the combined approach, the SPH's computational cost is superior to that of Lagrangian analysis, for single bullet model the duration for a single simulation is almost 3.5 times (133 min) more than a Lagrange equivalent.

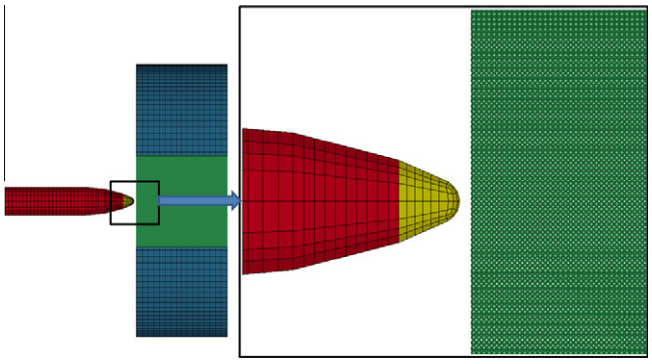

Fig. 11. SPH discretised target model.

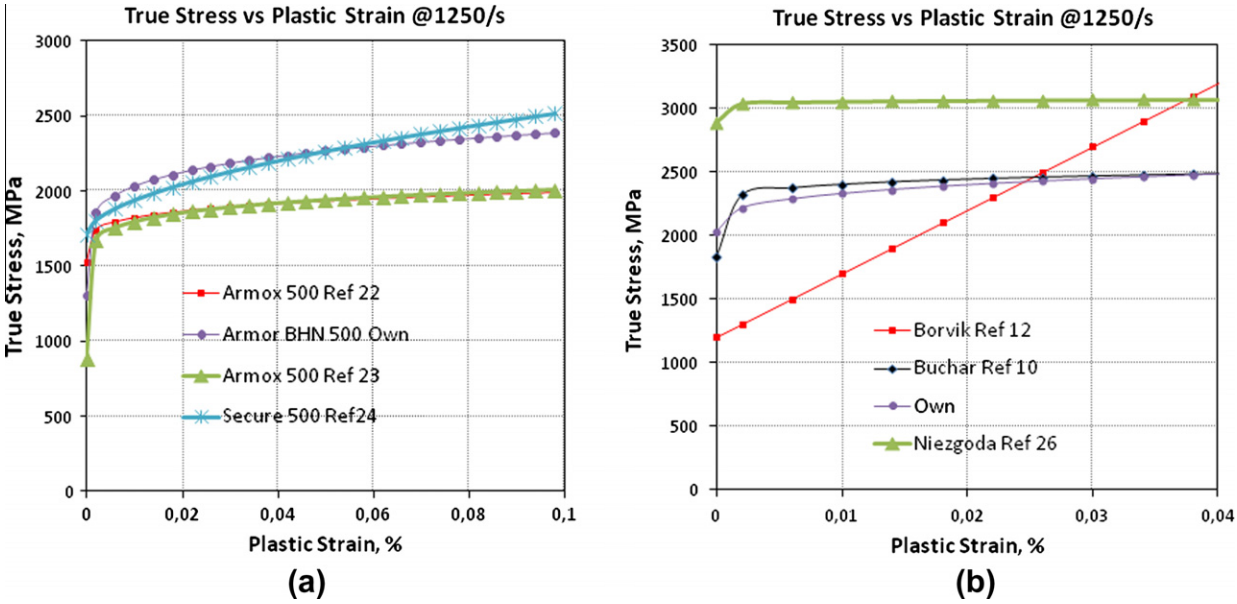

Fig. 12. Calculated stress–strain curves at strain rate 1250 s^{-1}: (a) for target material and (b) for steel core.

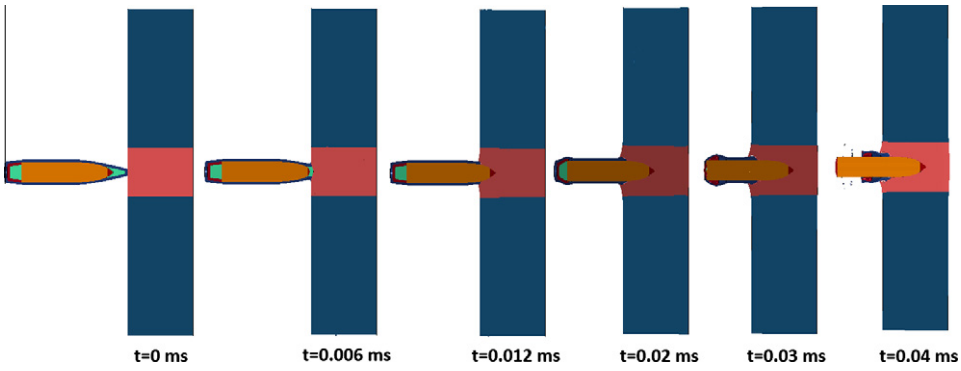

Fig. 13. Deformation plots for 20 mm target at various time steps.

4. Results and discussions

In the design of ballistic protection structures with explicit simulations, the success of numerical models is highly depend on some special features. First off all, the material description should be modeled accurately to exhibit realistic behavior during penetration. A list of J–C parameters for armor materials is tabulated in Section 2.1 [12,22–24]. Using the parameters found, the stress–strain curves at 1250 s^{-1} strain rate are visualized in Fig12a. The Armox 500T [22,23] and Secure 500 [24] armor steels have the nominal hardness value of 500 BHN and are valuable references to compare with own data since both of them are produced by similar manufacturing methods. It was shown that own armor steel is close to Secure 500. Even with the same hardness value, due to differences in chemical composition steels may show different behaviors at high strain rates. At least knowing that the magnitude of the found parameters are inline with literature for similar materials, all the concentration could be focused on numerical aspects to improve results. Similar approach is also valid for material model of hardened steel core. It was a great opportunity that both Borvik et al. [12] and Niezgoda and Morka [26] gave the hardness values found for steel core that a reasonable comparison can be done. As shown in Fig. 12b, the high strain rate behavior at 1250 s^{-1} is significantly different for each study but a close agreement is exist with Buchar et al. [10].

After eliminating the potential weakness coming directly from material development program, numerical simulations for the cases 9 mm and 20 mm have been carried out to examine if the computational model is able to predict the experimentally obtained target response, such as penetration depth, crater formation or residual velocity after penetration. In preliminary analysis, the bullet was modeled including brass jacket, lead antimony insert, clamped sabot and impacted on 20 mm target with initial velocity of 854 m/s. The results are plotted in Fig. 13. In the first phase (t = 0.006 ms) the brass jacket indents the target and lead–antimony insert is rapidly eroded. Damage on the target develops rapidly in the contact zone due to plastic straining of the elements close to projectile. As the material failed, in other words the damage reaches a critical value, elements are eroded which means no strength remains after erosion of an element. Element erosion was used to prevent overly distorted elements which reduce the drop of time step. If the time step drops a critical value, also element deletion is allowed to not further decrease. In preliminary analysis with smoothed radius steel core (see Fig. 9a), this

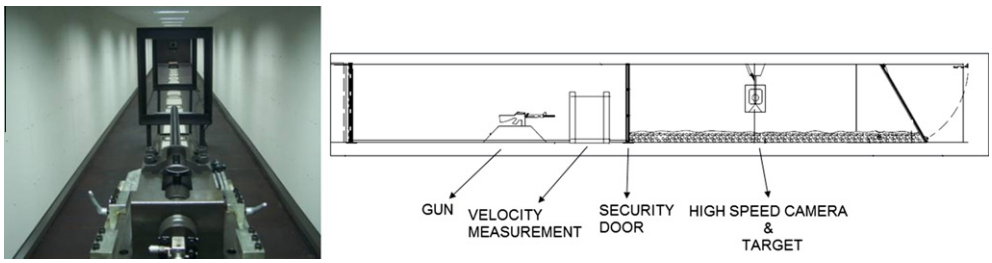

Fig. 14. Ballistic test setup.

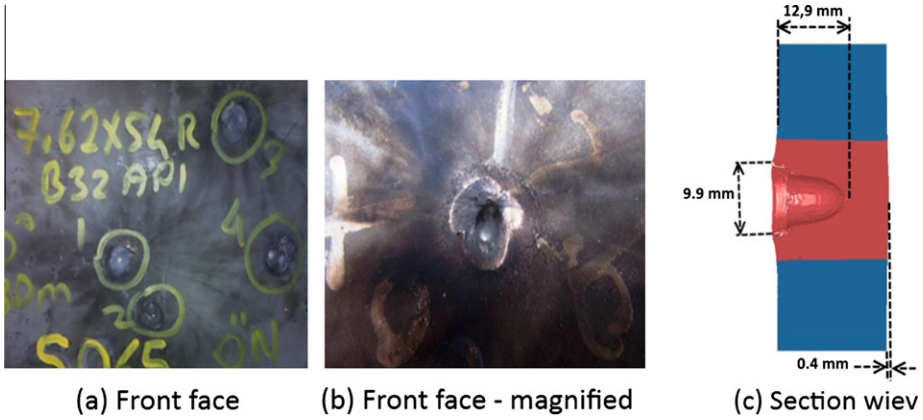

Fig. 15. Comparison with 20 mm thickness tests results.

approach eroded overly deformed elements of projectile, which decreased the penetration depth. With the novel approach, which includes rigid element tip, the element erosion does not happen.

The result were improved with finer mesh size especially in highly deformed region. The tendency of element erosion is increased with increasing mesh density, which means with decreasing mesh size the elements are more like to reach erosion criteria. Therefore the mesh size should not be decreased without control. The effect of friction between parts in contact have an effect on penetration depth. Although some of the reserachers have neglected friction to achieve conservative estimates on penetration [12], also there are studies that friction were taken into account. Borvik and his co-workers have studied the effect of friction and applied in penetration simulations. In this study, the effect of friction on penetration depth also investigated by keeping all other simulation parameters same. Penetration depth was predicted with various friction coefficients between 0 and 0.2 and the best results inline with shot tests were obtained with $\mu = 0.08$.

Ballistic tests were performed in the ballistics test laboratory in Otokar. The schematic representation ballistic test laboratory and a general view are given in Fig. 14. During the tests, with aluminum witness plate, the fragmentation and spall behavior of target are investigated and residual speed is measured using 42.000 fps high speed camera with 256×176 resolutions. Before each shot, the ammunition speed was adjusted with changing amount of powder in the cartridge to have a constant impact velocity of 854 m/s in accordance with Stanag 4569. The measured bullet velocity varies in ±20 m/s tolerance band for the five shots performed.

As stated before, with the J–C model predicted for the bullet steel core with material test program, the bullet appeared to be eroded prematurely and the penetration depth results are underestimated for 20 mm target (Fig. 7b). After increasing dynamic flow stress for hardened steel core, the results become more realistic and predict the depth of penetration with reasonable approximation. (Fig. 15). Founzoulas et al. [18] has experienced similar issue in modeling tungsten carbide sphere impact on high strength low alloy steel HSLA-100. With J–C parameters found by fitting the data from material tests, ammunition core appeared to fragment early and solved by modifying yield stress. Visual inspections of ammunition after shots have shown that bullet steel core are mainly broken into two or more pieces as shown in Fig. 16, which could not be simulated in numerical models. The dimensional integrity of steel core tip is successfully achieved. In tests, the depth of crater varies between 12.3 and 12.9 mm and the approximate diameter of crater varies between 13.1 and 15.5 mm. The agreement between the experimentally and numerically obtained penetration depths is excellent. Although the spall and cavity formation behavior is successively simulated, prediction is poor about crater diameter which is underestimated by 20%. For 20 mm target, the back face protrusion occurred and in simulations also the height is predicted well.

Fig. 16. Bullet parts after shot tests.

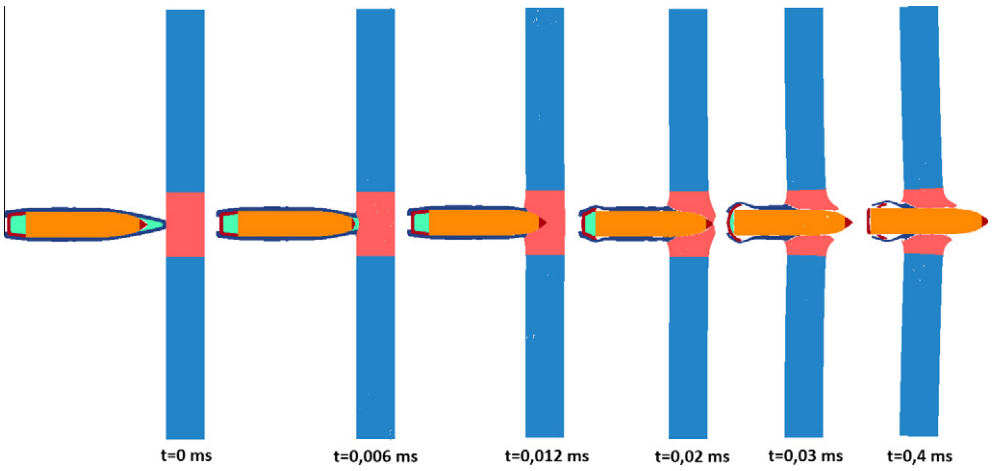

Fig. 17. Deformation plots for 9 mm target at various time steps.

Due to the stochastic nature of ballistics, in tests, bullets will not cause a perpendicular penetration. Only one of five shots, the deformation on target shows perpendicular bullet intrusion and rest of them show oblique patterns. One of the reasons of underestimation of crater diameter may be oblique nature of shots. A weakness of the performed simulations is literature dependent jacket and lead cap material models. In most of the studies about ballistic simulation, only penetration depth was become main subject of the study, therefore there is not much information on comparison of penetration patterns.

In order to increase confidence of the simulation parameters, additional shots performed on 9 mm plate with same initial bullet velocity. The numerical results during perforation are plotted for various time steps in Fig. 17. The residual velocity after penetration is monitored with high speed camera to compare with simulation results. The measured residual velocity in test is 487 m/s which predicted in numerical analysis as 455 m/s. As shown in Fig. 18c, the spall behavior and perforation of armor is successively simulated.

Due to numerical cost of full model, most of the studies with AP projectiles were performed using only steel hardened core. A valuable study about the effect of jacket and lead cap on perforation resistance was studied by Borvik and his co-workers [12]. In their experimental study, both jacket and cap removed from AP bullet and hardened core was inserted in a sabot. By removing the jacket and cap, the mass is decreased from 10 to 5 g. It was shown that the ballistic limit velocity was decreased only by 3–5% when only hard core is used as projectile. This really important observation indicates that, modeling only core without jacket and caps will not cause significant differences in simulation results. Before dealing with ballistic limit studies for various thicknesses of high hardness armor steel, we would like to simulate same observation numerically. In order to visualize this, by keeping all parameters same in simulation only cap and jacket was removed. Two separate criterion used to setup a correlation between full bullet and hardened steel core simulations; penetration depth and residual velocity. Although general observation is in line with the Borvik et al. [12], the differences are found to be up to 10% in penetration depth (Fig. 19b and c) when target thickness is increased. For moderate thicknesses 10–15 mm, (Fig. 19a) differences are between 4% and 5% which is still more than Borvik's results. The outcome for residual velocity is quite different. Simulations with only core model show significantly poor correlation in residual velocity close to ballistic limits.

The scope of this study is to demonstrate that, with Lagrange and SPH discretization, the ballistic limit thickness of high hardness steel armor against Stanag 4569 level 3 threat can be predicted. The full bullet Lagrangian model takes approximately 136 min to complete single simulation on 16 CPU, hardened core Lagrange model takes only 38 min. With hardened core model the numerical cost significantly decreases. Since the difference in penetration depth between full bullet and steel core model is only ~4–10%, in ballistic limit determination studies, only steel core model will be used. The numerical cost of SPH discretization is significantly high when compared with Lagrangian ones. Even with single bullet model simulation takes 133 min for single run. For the thin target, mostly hardened steel core penetrates and pass with a residual velocity. When compared with penetration depth for full and single core projectile, residual velocity difference is not predictable in magnitude. Mainly incident velocity versus residual velocity plots widely used in ballistic limit determination, but in this study we will follow performance of armor by considering only penetration depth up to full penetration.

A comparison between discretization methods is presented in Fig. 20. Numerical results at various time steps during penetration of bullet are plotted for both SPH and Lagragian models. At the same time interval, the residual velocity with SPH found to be more than what Lagrange approach is predicted. In general, from

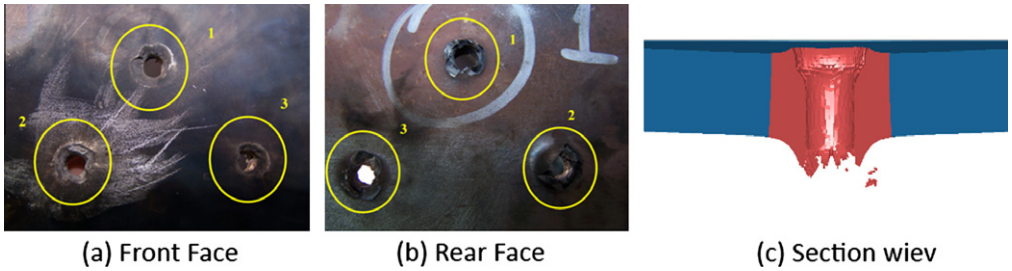

Fig. 18. Comparison with 9 mm thickness tests results.

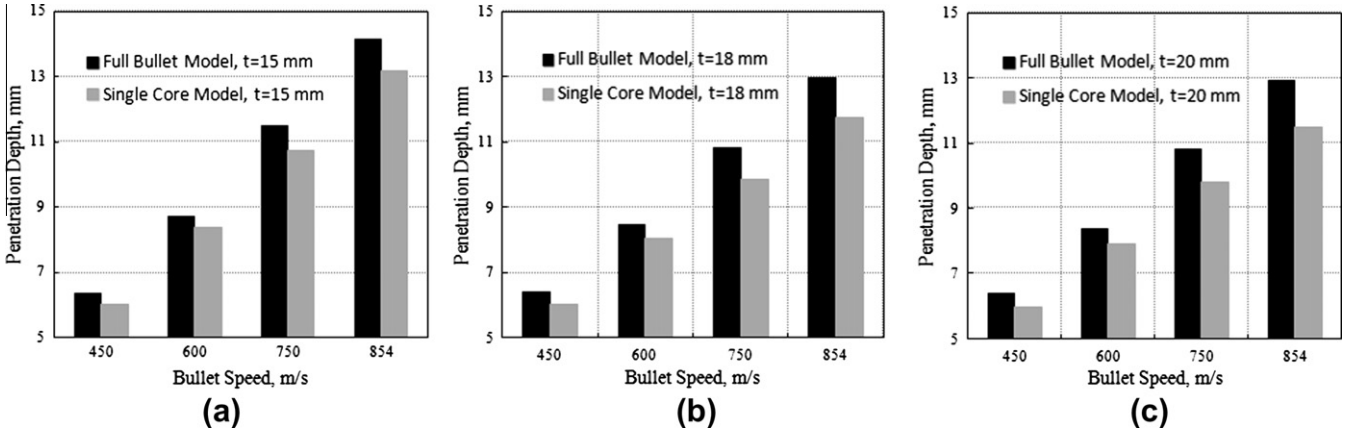

Fig. 19. Full bullet modeling affect on penetration depth for various thicknesses: (a) 15 mm, (b) 18 mm and (c) 20 mm target.

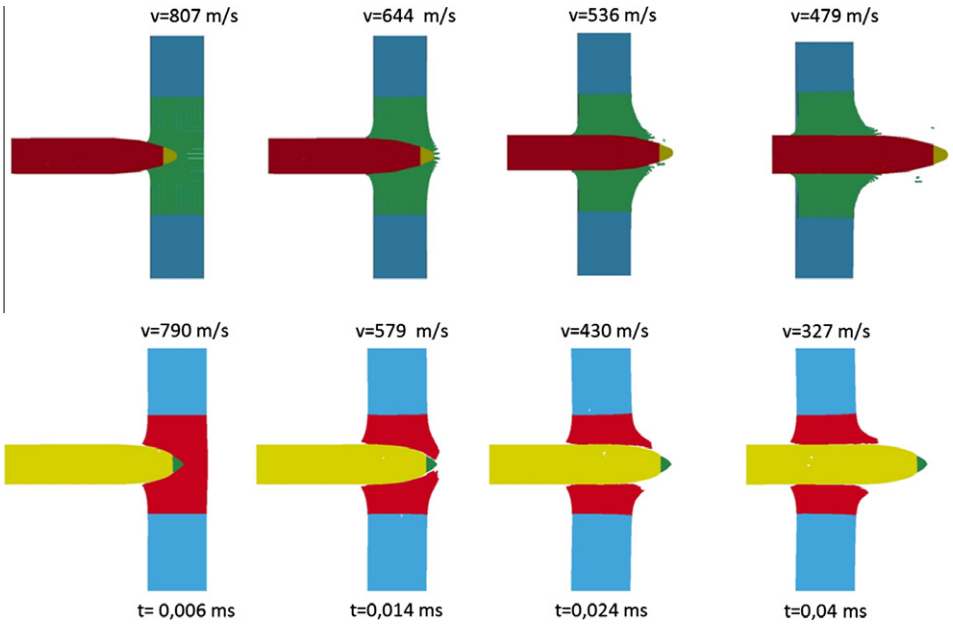

Fig. 20. Deformation plots for penetration of 9 mm armor. 1st row SPH and 2nd row Lagrange discretization.

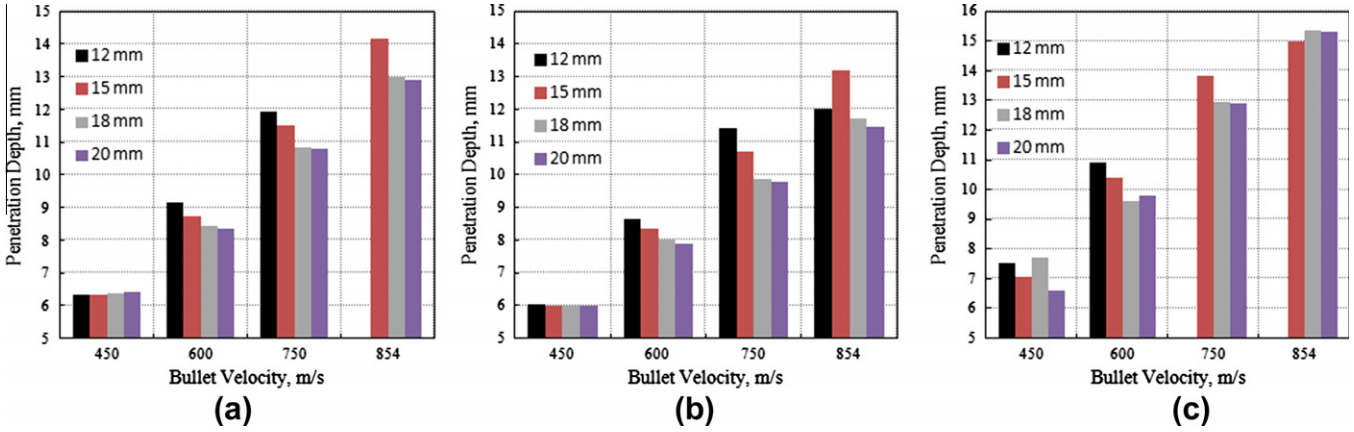

Fig. 21. Ballistic limit thickness for Stanag 4569 level 3 threat: (a) full bullet model with Lagrange discretization, (b) steel core model with Lagrange discretization and (c) steel core model with SPH discretization.

penetration depth point of view results with SPH methods are less than Lagrange ones due to the sharp tip model could not be implemented in SPH models. Although, common knowledge about using SPH methodology has benefit on representing spall and fragmentation behavior more accurately, results show that, there is not a significant difference. Lagrange model seems more successful in simulation of fragmentation and material deformation.

From the simulations, the numerical model seems to capture the perforation behavior during the penetration and promising results are obtained to determine ballistic limit thickness. In order to determine ballistic limit, 24 runs performed for each model. As shown in Fig. 21a, ballistic limit against Stanag 4569 level 3 was determined for full bullet model as 14.5 mm. In Demir and his co-worker's experimental study, ballistic impact behavior of various hardness steels against 7.62 mm armor piercing projectile was investigated [31]. Projectile used in tests is 100Cr6 which has a hardness value of 62 HRc (748 HV) which is approximately 80 HV lower than our case. One of the target materials they used has 528 BHN harness value which can be a good comparison to verify whether found ballistic limit is reasonable or not. They have found that for 782 m/s projectile velocity, approximately with 100 kg/m^2 areal density which is equal to 12.4 mm thickness, projectile was achieved to stop. In our simulations, the ballistic limit for 12.4 mm thickness was found about 775 m/s. In hardened steel core simulations, the ballistic limit is found to be 13 mm for Lagrange and 15.5 mm for SPH discretization. It is interesting to see that, in all cases increasing target thickness will decrease penetration depth up to ballistic limit. When the target thickness is more than ballistic limit, the penetration depth does not show any dependency on target thickness.

5. Conclusions

In this study, the perforation resistance of high hardness steel against 7.62 mm armor piercing bullet has been determined numerically and compared with experimental results. The numerical models developed using Lagrange and SPH discretization to simulate complex fragmentation behavior. To be able to simulate the material behavior taking place during penetration, characterization of the target material and ammunition steel core under high strain rate load condition was determined with a material test program. According to numerical and experimental data developed during the study, the following main conclusions can be drawn:

- The Johnson–Cook material model derived for target material is capable to characterize spall behavior during penetration. The material model has similar parameters when compared with the available literature based data for steels which have hardness around 500 HB.
- The Johnson–Cook material model derived for bullet core needs further improvement. The main reason of not achieving a reasonable model is no doubt, the difficulties experienced during preparing miniature specimens. The strain rate parameters in bullet J–C model were modified to eliminate premature erosion of bullet tip during simulations. The modified model is sufficient since the main objective of the study is to predict ballistic resistance thickness but even with modified material model, projectile fracture during penetration could not be simulated.
- The simulation results are found to be sensitive to the equation of state formulation used and best approximation is achieved with Mie-Gruneisen EOS.
- The numerical simulation results with Lagrangian formulation of full bullet model shows good agreement with test results. The results were improved with finer mesh size especially in highly deformed region. The tendency of element erosion is increased with increasing mesh density, which means with decreasing mesh size the elements are more like to reach erosion criteria. Therefore the mesh size should not be decreased without control. The developed numerical model can be used for ballistic thickness prediction with high confidence.
- Due to numerical cost of full bullet simulations, in ballistic limit thickness determination, simulations were carried out using only the steel core of the armor piercing bullet. It was found that when only the steel core was used as projectile, the ballistic limit thickness is decreased by 7%. This outcome indicates that it is reasonable to model only steel core in ballistic limit calculations.
- Although, with SPH formulation it is expected to predict spall and fragmentation behavior more accurately, there is not a significant difference found. A finer particle size for the SPH method would not have predicted the experimental data more accurately, since SPH mesh convergence studies have shown that penetration depth is not a function of particle size. Even a hybrid SPH modeling used to decrease numerical cost, still SPH is too costly when compared with Lagragian formulation.

Acknowledgments

The authors would like to thank Technology and Innovation Funding Programs Directorate and Otokar Otomotiv ve Savunma Sanayi A.S. for their financial support of the research project TEYDEB:3060493 that forms the basis of this work and support from Prof. Dr. Orhan Yıldırım and Atıl Erdik for the preliminary analysis performed. Furthermore, the authors would like to acknowledge Prof. Mustafa Guden and Ass. Prof. Alper Taşdemirci from İYTE Dynamic Test Laboratory for the material test program carried out.

References

[1] Bangash MYH. Shock impact and explosion structural analysis and design. Springer; 2009.
[2] Zukas JA, Nicholas T, Swift HF, Greszczuk LB, Curan DR. Impact dynamics. New York: J. Wiley; 1982.
[3] LS-Dyna keyword user's manual version 971. Livermore Software Technology Corporation (LSTC); 2007.
[4] Abaqus theory manual, version 6.7.
[5] MSC.DYTRAN theory manual version. MSC.Software Corporation; 2005.
[6] Sph user manual & tutorial, revision 4.3. Century Dynamics Inc; 2005.
[7] Donea J, Huerta A, Phontot J, Ferran AR. Arbitrary lagrangian eulerian methods. Encyclopedia of computational mechanics, vol. 1. John Wiley & Sons; 2004.
[8] Liu GR. Mesh free methods. Florida CRC Press; 2003.
[9] Vesenjak N, Ren Z. Application aspects of the meshless SPH method. J Serb Soc Comput Mech 2007;1:74–86.
[10] Buchar J, Voldrich J, Rolc S, Lisy J. Ballistic performance of dual hardness armor. In: 20th International symposium on Ballistics Orlando; September 2002. p. 23–27.
[11] Li J, Li XJ, Zhao Z, Ou YX, Jiang DA. Simulation on projectile with high rotating speed penetration into the moving vehicular door. Theoret Appl Fract Mech 2007;47:113–9.
[12] Borvik T, Dey S, Clausen AH. Perforation resistance of five different high-strength steel plates subjected to small arms projectiles. Int J Impact Eng 2009;36:948–64.
[13] Dey S, Borvik T, Teng X, Wierzbicki T, Hopperstad OS. On the ballistic resistance of double –layered steel plates: an experimental and numerical investigation. Int J Solids Struct 2007;44:6701–23.
[14] Borvik T, Olovsson L, Dey S, Langseth M. Normal and oblique impact of small arms bullet on AA6082-T4 aluminum protective plates. Int J Impact Eng 2011;38:577–89.
[15] Dey S, Borvik T, Hopperstad OS, Langseth M. On the influence of fracture criterion in projectile impact of steel plates. Comput Mater Sci 2006;38:176–91.
[16] Khoda-rahmi H, Fallahi A, Liaghat GH. Incremental deformation and perforation analysis of deformable projectile into semi-infinite target. Int J Solids Struct 2006;43:569–82.
[17] Aktay L, Johnson AF, Kroplin BH. Combined FEM/Meshfree SPH method for impact damage predictions of composite sandwich panels. ECCOMAS thematic conference on meshless methods; 2005: D13.1-6.

[18] Fountzoulas CG, Gazonas GA, Cheeseman BA. Computational modeling of tungsten carbide sphere impact and penetration into high strength low alloy HSLA-100 steel targets. J Mech Mater Struct 2007;2:1965–79.
[19] Buyuk M, Kan SCD, Bedevi NE, Durmus A, Ulku S. Moving beyond the finite elements, a comparison between the FEM and meshless methods for a ballistic impact simulation. In: 8th International LS-DYNA users conference; 2004.
[20] Johnson GR, Cook WH, A constitutive model and data for metals subjected to large strains, high strain rates and high temperatures. In: Proceedings of the 7th international symposium on ballistics, Hauge; 1983. p. 541–547.
[21] Kurtaran H, Buyuk M, Eskandarian A. Ballistic impact simulation of GT model vehicle door using finite element method. Theoret Appl Fract Mech 2003;40:113–21.
[22] Skoglund P, Nilsson M, Tjernberg A. Fracture modeling of a high performance armour steel. J Phys IV France 2006;134:197–202.
[23] Nilsson M. Constitutive model for Armox 500T and Armox 600T at low and medium strain rates. FOI, Swedish Defence Research Agency, TR FOI-R-1068-SE; 2003.
[24] Nsiampa N, Coghe F, Dykmans G. Numerical investigation of the bodywork effect. DYMAT 2009:1561–6.
[25] Chocron S, Anderson CE, Grosch D, Popelar CH. Impact of the 7.62 mm APM2 projectile against the edge of a metallic target. Int J Impact Eng 2001;25:423–37.
[26] Niezgoda T, Morka A. On the numerical methods and physics of perforation in the high-velocity impact mechanics. World J Eng. p. 414.
[27] Jutras M. Improvement of the characterization method of the Johnson–Cook model. M.Sc. thesis Université Laval. Québec City – Canada; 2008.
[28] Espinosa HD, Dwivedi S, Zavattieri PD, Yuan G. A numerical investigation of penetration in multilayered material/structure systems. Int J Solid Struct 1998;35:2975–3001.
[29] Gailly A, Espinosa HD. Modelling of failure mode transition in ballistic penetration with a continuum model describing microcracking and flow of pulverized media. Int J Numeric Methods Eng 2002;54:365–98.
[30] Azavedo RL, Alves M. Numerical simulation of soft body impact on GFRP laminate composites mixed SPH-FE and pure SPH approaches. Mech Solids Brazil 2009;1–2:15–30.
[31] Demir T, Übeyli M, Yıldırım RO. Investigation on the ballistic impact behavior of various alloys against 7.62 mm armor piercing projectile. Mater Des 2008;29:2009–16.